Hong Kong J Radiol. 2017;20:6-16 | DOI: 10.12809/hkjr1716836

REVIEW ARTICLE **CME**

State-of-the-art Musculoskeletal Magnetic Resonance Imaging: Technical Review

L Xiao[1], MK Yuen[2]

[1]Medical Physics Unit, Department of Oncology, and [2]Department of Radiology, Tuen Mun Hospital, Tuen Mun, Hong Kong

ABSTRACT

Magnetic resonance imaging (MRI) has been used widely in the diagnosis and treatment of musculoskeletal (MSK) disorders. Innovative MRI techniques have been developed for MSK imaging. This review discusses the advantages and challenges of the cutting-edge technology of MSK MRI (both hardware and software) as well as its clinical application.

Key Words: *Imaging, three-dimensional; Magnetic resonance imaging; Prostheses and implants*

中文摘要

肌肉骨骼磁共振成像最新技術進展

肖麗、袁銘強

磁共振成像已廣泛用於診斷肌肉骨骼疾病。新穎磁共振成像技術也嘗試應用於肌肉和骨骼。本文複習討論新穎磁共振成像技術（包括硬體和軟件）應用於肌肉和骨骼的優勢和挑戰。

INTRODUCTION

In the past 30 years, imaging technology has revolutionised almost every aspect of medical care. Primary care physicians or family doctors as well as medical and surgical subspecialists rely heavily on imaging to establish early and accurate diagnosis, triage to an appropriate specialist, and plan and monitor treatment. In developed countries, musculoskeletal (MSK) disorders are the leading cause of disability, accounting for more than one-half of all chronic conditions in people over 50 years of age. Due to its excellent soft-tissue contrast and multiplanar capabilities, magnetic resonance imaging (MRI) plays a vital role in the evaluation of the anatomy of the MSK system and abnormalities. Advances in MSK imaging depend on improvement in both MRI hardware and software. Standard structural MRI sequences (including T1- and T2-weighted spin-echo and fast spin-echo, [spoiled] gradient-echo, and contrast-enhanced images) provide most information. Advanced techniques, however, can provide more detailed physiological or anatomic information that increases sensitivity and

Correspondence: *Dr Li Xiao, Medical Physics Unit, Department of Oncology, Tuen Mun Hospital, Tuen Mun, Hong Kong. Email: xl430@ha.org.hk*

Submitted: 30 Dec 2016; Accepted: 20 Feb 2017.

Disclosure of Conflicts of Interest: All authors have disclosed no conflicts of interest.

specificity of diagnosis and guides management.

DIGITAL REVOLUTION IN MAGNETIC RESONANCE IMAGING

In the last two decades, MSK MRI has benefited from the introduction of phased array coil technology.[1] By combining multiple small coils into large arrays, both high signal-to-noise ratio (SNR) and large fields of view can be obtained. In principle, *N* independent phased array coils, each with their own amplifiers and receiver channels, ideally increase SNR by a factor of $\sqrt{N}$, although practical gains are usually below the maximum allowed. With the introduction of parallel imaging,[2-4] the number of phase-encoding steps is reduced to speed up imaging with information about coil positions and sensitivities, and thus the scan time and the number of radiofrequency pulses required to form an image are reduced (Figure 1). This can limit the total radiofrequency power and specific absorption rate in line with regulatory guidelines. In addition, susceptibility artefacts and phase-related distortions can be lessened with a shorter echo time. Because the strategy of parallel imaging depends on estimation of the spatially varying sensitivity profiles of receiver coil elements to reconstruct the final image, image-processing-related artefacts are present and non-uniformly distributed. Reconstruction errors can be reduced with the increased number of receiver coil channels. The design and configuration of array coils and the move towards higher channel counts in coils to accommodate parallel imaging methods have evolved over the last two decades. The number of receiving channels in the system has increased substantially up to 32.[5] Coil elements are cheap to produce. Nonetheless, additional long-receiving cables between coil elements and the MRI data acquisition system with traditional analogue technology are required to support more and more channels. These analogue cables with their bulky connectors and associated electronics for multiplexing, complex switching logic, and dynamic range compression can make the system extra sensitive to noise pick-up, which in turn deteriorates image quality. With the advances in analogue-to-digital signal conversion, the newest MRI systems can use small high-frequency analogue-to-digital converters in close proximity to the coils to allow direct digital sampling of signals and send the digitised data via fibre-optic cables. This avoids all intermediate analogue stages for down-conversion of the signal between coil elements and analogue-to-digital converters. The MRI signal is sampled directly without conversion to direct current (zero frequency) and transported in digital format. Digitisation in the receiver coil miniaturises the receiving electronics. The overall result of digital revolution in MRI is an incredibly simplified receiving architecture, with substantially fewer components, lower power consumption, higher SNR and dynamic range that improve overall signal fidelity and signal-and-phase stability. Figure 2 compares the SNR of digital architecture and traditional architecture with the same scan parameters. These advantages help clinicians make informed decisions in the evaluation of MSK diseases.[6-9] Bone structure, cartilage, tendons, and ligaments are more clearly imaged and pathology more easily

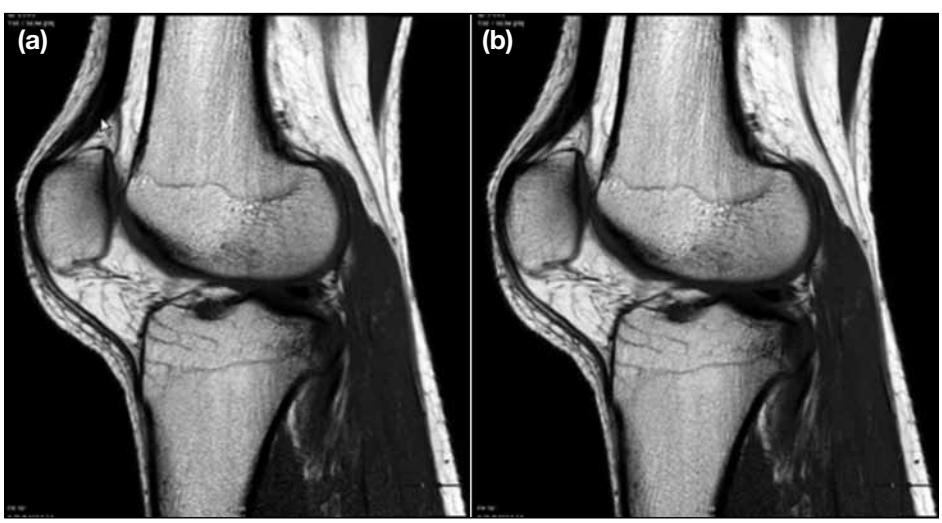

Figure 1. Sagittal T1-weighted fast spin-echo images acquired at 1.5 T (a) with and (b) without SENSE, with all other parameters being identical, showing a slightly lower signal-to-noise ratio in the image with SENSE. The whole scan time is 1:29 and 2:55 minutes, respectively.

Figure 2. Images acquired at (a) digital 1.5 T and (b) analogue 1.5 T with identical scan parameters showing a 42% improvement in the signal-to-noise ratio in the image with digital architecture (images courtesy of Philips).

detected.[10-12] The increased performance provides a more accurate assessment of bone marrow and adjacent soft tissue infiltration and enables reliable visualisation of marrow components and precise evaluation of tumour staging and recurrence. The increased SNR enables clearer images with previously unseen details as well as better resolution or faster scans. Moreover, the advent of digital revolution in MRI has increased the feasibility of whole-body MRI without considerable compromise of spatial resolution. Whole-body MRI is particularly important in detecting skeletal metastases, of which up to 40% are outside the field of view of a routine skeleton assessment.[13-15] Digital MRI provides a reliable, patient-friendly approach in the realm of oncology imaging, staging, and treatment assessment.

REDUCTION OF ARTEFACTS FROM METALLIC IMPLANTS

Metallic implants in the ageing population are common. It is important to use the appropriate imaging modalities for preoperative planning, postoperative patient monitoring, and evaluation of implants.[16] Due to its sensitivity for soft tissue abnormalities and marrow oedema, MRI generally provides better results for patients with orthopaedic implants. Metallic implants with high magnetic susceptibility, however, lead to distortion and formation of areas of signal loss or abnormally high signal. In order to reduce artefacts related to metallic implants and optimise MRI, factors that contribute to artefacts and their related theories and artefact reduction techniques should be understood.

Susceptibility (χ) is a measure of the extent to which a substance becomes magnetised when placed in an external magnetic field, which is fundamental to MRI.[17] Field distortions and susceptibility artefacts are usually prominent around metal objects because metals have very high intrinsic magnetic susceptibility (χ) that produces significant local field disturbances with both in-plane and through-plane changes in resonance frequency. By changing resonance frequencies, the significant susceptibility differences shift image pixels away from their true position leading to significant geometric distortions including signal voids (black areas) and signal pile-ups (bright areas). The shape and intensity of the artefact are related to field strength, echo time (TE), bandwidth, local anatomic relationships, and difference in susceptibility:

$$susceptibility \times artefacts \times size \propto \frac{(\Delta susceptibility) \times B_0 \times TE}{bandwidth}$$

According to the above equation, simple modifications can optimise imaging around metal implants independent of the protocol used.[18-20] Scanning at a higher magnetic field should be avoided in patients with metal implants because of worse susceptibility artefacts. Susceptibility artefacts can be minimised by using shorter TE to avoid serious dephasing. Decreasing the slice thickness and voxel size also reduces artefact size. Susceptibility artefacts can also be minimised by increasing gradient strength for a given field-of-view and avoiding a narrow bandwidth, as well as using parallel imaging acceleration. Spin-echo protocols are preferred to gradient echo protocols, as the local inhomogeneity caused by rapid dephasing can be rephased in spin echo. Aligning implants with the main magnetic field further reduces artefact size. Figure 3 shows the improvement using basic metal artefacts reduction techniques.

Fat suppression can improve detection of bone marrow oedema and marrow lesions, confirm or exclude the presence of fat in soft tissue tumours, differentiate

fat from met-haemoglobin, protein-rich fluids and / or melanin, eliminate chemical shift artefacts (that are challenging mainly on 3T MRI), and is essential in T1-weighted post-contrast imaging and MR arthrography. There are two main types of fat-suppression techniques (Table 1). The first is based on the chemical shift phenomenon between protons of water and fat (difference between water and fat is 220 Hz @1.5 T and 440 Hz @3.0 T, respectively) including pulse-selective saturation techniques (fat saturation) and phase-shifts techniques (water excitation, ProSet, Dixon, etc).[21-24]

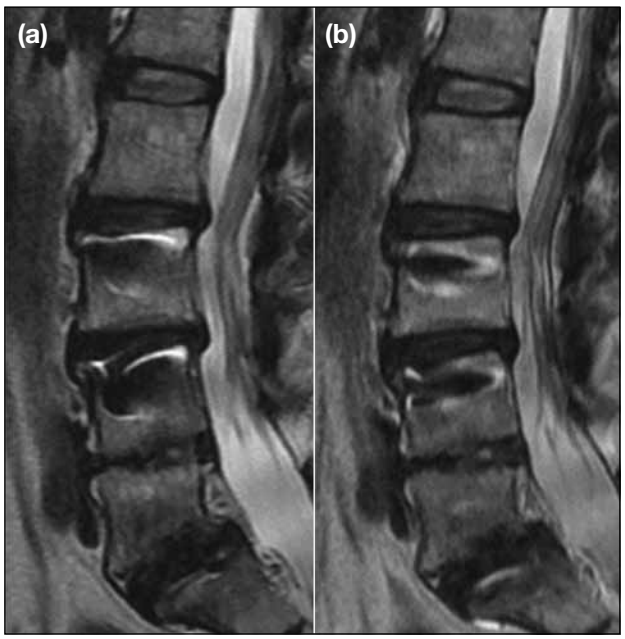

Figure 3. T2-weighted sagittal images of the spine showing (a) metallic susceptibility artefacts from screws, and (b) artefacts decreased by metal artefact–reduction techniques using a spin-echo pulse sequence with short echo spacing, maximising receiver bandwidth with acceptable level of signal-to-noise ratio, and reducing slice thickness with parallel imaging acceleration.

The second is based on T1 relaxation time and uses inversion recovery techniques such as short-TI inversion recovery (STIR) pulse,[25] spectral presaturation with inversion recovery (SPIR), and spectral-attenuated inversion recovery (SPAIR). The latter two are a hybrid of both fat-suppression techniques. Appropriate choice of fat-suppression technique may reduce the chance of failure. As STIR is less sensitive to magnetic field inhomogeneity, it provides much more homogeneous fat suppression and better results than conventional fat-saturation techniques, especially near metallic implants (Figure 4). There are limitations to STIR. STIR is not a suitable fat-suppression technique when a contrast agent is used; it suppresses tissues with a T1 value in the range of fat (200-300 ms) as well as contrast-enhanced tissues with similar relaxation times. In addition, the overall SNR may be poor. Dixon techniques might provide better results for contrast-enhanced imaging in the presence of metal implants (Figure 5).[26]

The significant improvement of MRI around metallic implants may be accomplished by specific metal artefact reduction pulse sequences. Several MR vendors offer specially designed pulse sequences to minimise metal artefacts.

View angle tilting (VAT) is used to substantially reduce in-plane image distortions caused by susceptibility artefacts.[27] It applies a compensation gradient during signal readout along the slice-selection direction. The amplitude of the gradient is equal to the slice-selection gradient. All excited spins within the radiofrequency bandwidth are re-registered and local off-resonance effects are cancelled. The effect of the design is as though the slice is viewed at a titled angle. The clinical application of VAT includes assessment of periprosthetic soft tissues after hip joint replacement surgery, postoperative assessment after resection of

Table 1. Major types of fat-suppression techniques.

Fat-suppression technique	Time penalty	Specific absorption rate	Sensitivity to B_0	Sensitivity to B_1
Chemical shift based				
Chemical shift selective imaging sequence / fat saturation	Small	Medium	High	High
Water excitation	Small	Low	High	Low
Dixon techniques	Large	Low	Low	Low
Inversion based				
Short-TI inversion recovery	Large	High	Low	Low
Hybrid				
Spectral presaturation with inversion recovery	Medium	Medium	High	High
Spectral-attenuated inversion recovery	Large	High	High	Low

bone tumours and reconstruction, and localisation of non-opacified methyl methacrylate cement prior to hip arthroplasty revision surgery.[28] Although VAT is robust to in-plane distortions, it results in image blurring and through-plane distortions. To further suppress the through-plane artefacts due to metal implants, slice encoding for metal artefact correction (SEMAC)[29] and multi-acquisition variable resonance image combination (MAVRIC)[30] have been developed (Figure 6). Based on the VAT method, the SEMAC technique corrects metal artefacts by extending the VAT sequence with additional phase encoding steps along the slice selection direction. This resolves metal-induced inhomogeneities that distort the original slice profile. During image reconstruction, the shifted spins are located back to their actual positions and correct the through-plane distortions. The MAVRIC technique is based on conventional three-dimensional (3D) fast spin-echo sequences. It acquires multiple overlapping volumes at discrete frequency offsets. It uses a multispectral VAT-type readout. A spectrally correlated de-blurring technique is implemented to remove artefacts from the final composite image. Both the partial Fourier technique and parallel imaging technique are compatible with SEMAC and MAVRIC and can decrease examination time.

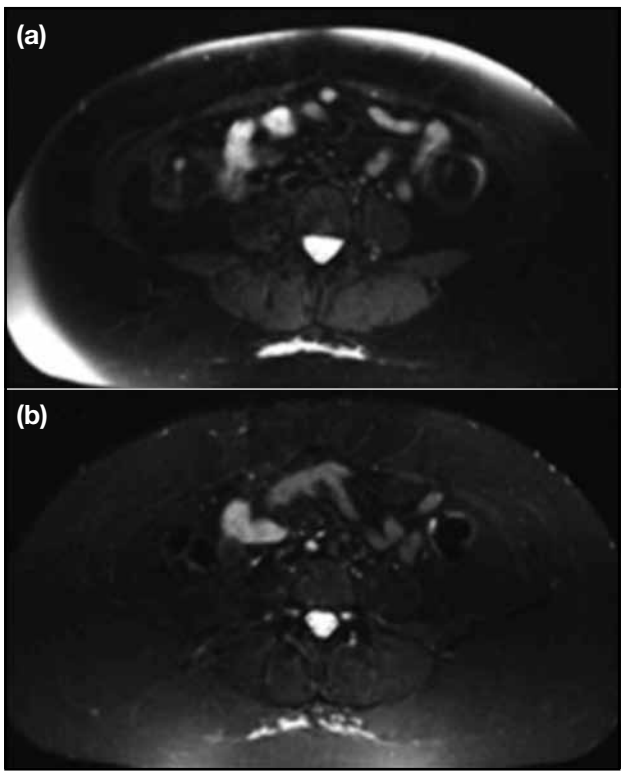

Figure 4. (a) Axial T2-weighted spectral-attenuated inversion recovery image showing heterogeneous suppression of fat, a result of B_0 inhomogeneity at the edge of the large field of view. (b) Axial short-TI inversion recovery image showing better homogeneous suppression of fat, especially near metallic implants, compared with conventional fat-saturation techniques.

Metal artefact–reduction techniques reduce the size and intensity of susceptibility artefacts, improve visualisation of structures adjacent to implanted metal staples, pins, or screws, and enable better assessment of postoperative complications.

RAPID THREE-DIMENSIONAL IMAGING

The two-dimensional fast spin-echo (2D FSE) technique is commonly used in MSK imaging due

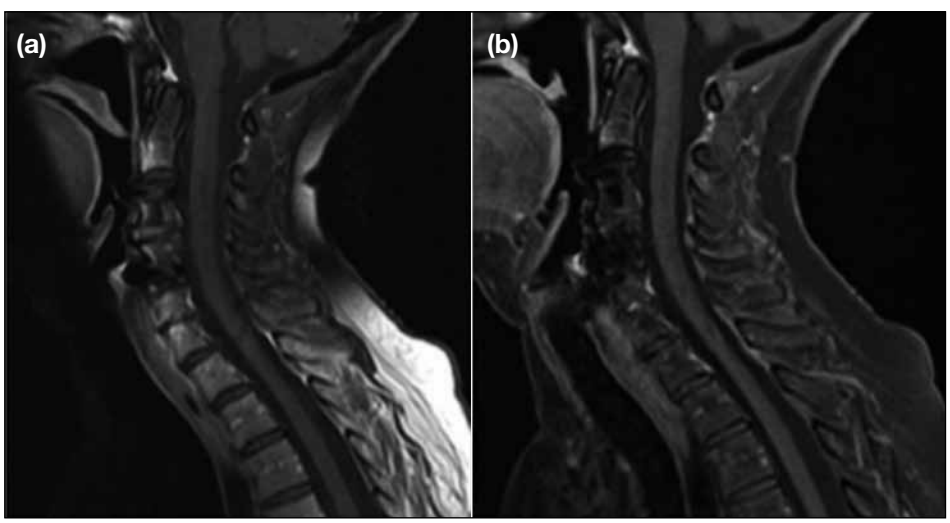

Figure 5. Sagittal T1-weighted images of the cervical spine using (a) conventional fat-saturation techniques that result in heterogeneous saturation of the fat in the posterior side of the neck, and (b) the Dixon technique (Siemens, Erlangen, Germany) that results in robust fat suppression and better contrast-enhanced image in the presence of metal implants (images courtesy of Siemens).

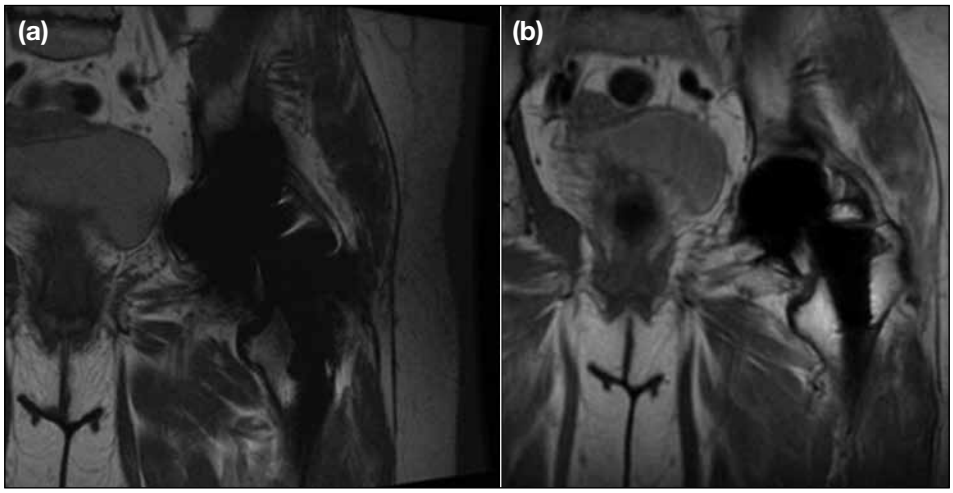

Figure 6. Coronal T1-weighted images of the hip using (a) two-dimensional fast spin echo with basic metal artefact reduction techniques, and (b) the multi-acquisition variable resonance image combination technique that results in noticeable artefact reduction (images courtesy of GE).

to its excellent soft-tissue contrast. It offers excellent direct depiction of anatomy and pathology, including ligamentous and cartilaginous structures,[31,32] meniscal tears,[33,34] bone marrow, fibrous, and periarticular soft tissue. Nonetheless, many anatomical structures such as ligaments and tendons are obliquely orientated and are difficult to assess with 2D sequences orientated in the standard planes. With a standard slice thickness of 3-5 mm, the voxels obtained are anisotropic and prevent the images from being reformatted into various oblique planes. The depiction is also often affected by partial volume effects due to relatively thick slices and interslice gap, which may mimic signal alteration and result in inaccurate quantification of cartilage volume and other structures. Isotropic 3D sequences can overcome the drawbacks of 2D sequences in visualisation of anatomy, pathology, and cartilage quantification. They improve through-plane spatial resolution and reduce partial volume artefacts as a result of the thin contiguous slices. This potentially enhances their ability to detect subtle lesions that might be overlooked with standard 2D sequences. Moreover, 3D isotropic sequences enable retrospective reformatting of high-quality images from original data acquisition into any arbitrary plane for better visualisation of oblique anatomy,[35-37] without any time penalty. With the ability of post-processing multiplanar reformatting from only one acquisition, the scan time of isotropic 3D sequences is reduced, compared with multiplane acquisitions with 2D sequences. The latest higher-field strength MRI system, high performance gradients, multi-channel extremity coils, parallel imaging technique, and direct digital sampling of signals facilitate time-efficient acquisition with 3D isotropic imaging in routine practice. Gradient-echo and fast spin-echo sequences have been used in clinical practice.[38] 3D gradient echo pulse sequences are commonly used to assess articular cartilage.[39-41] Potential disadvantages of gradient-echo 3D sequences include inherent sensitivity to susceptibility artefacts and intravoxel dephasing. Moreover, the MSK tissue contrast characteristics differ between 3D gradient echo imaging and 2D fast spin-echo sequences when assessing joints. Therefore, clinical application of gradient-echo 3D sequences might be limited. 3D FSE sequences are developed to more closely match the image contrast characteristics of 2D FSE sequences and to be more robust to susceptibility artefacts.[42-44] Nonetheless, they have a long scan time or low SNR. Technical advances in MRI hardware and software have enabled 3D FSE MSK MRI to achieve a reasonable scan time with good image quality. The average examination time is 6-10 minutes per 3D FSE sequence depending on the organ of interest and the size of the joint.[45,46] Isotropic 3D FSE sequences are effective to assess MSK pathologies (Table 2 and Figure 7).

T2 / T2* MAPPING FOR CARTILAGE ASSESSMENT

Conventional morphological MRI sequences such as T1- and T2-, proton density–weighted sequences form the basis of diagnosis, staging, and follow-up of MSK disorders. Nonetheless, morphological MRI may not be able to detect early, subtle, or slow biochemical

Table 2. Commonly used three-dimensional (3D) pulse sequences in musculoskeletal magnetic resonance imaging.

Type of sequence	Naming conventions			Fluid signal intensity
	Siemens	Philips	GE	
Spin echo				
3D fast spin echo	Sampling perfection with application optimised contrasts using different flip angle evolution (SPACE)	Volume isotropic turbo spin echo acquisition (VISTA)	CUBE	Available for T2-, T1-, or proton density–weighted, FLAIR or IR images
Gradient echo				
Steady-state free precession (SSFP)-FID	FISP	FFE	GRASS	High
SSFP-echo	PSIF	T2-FFE	SSFP	High
SSFP-double	DESS		MENSA	High
SSFP-balanced	True FISP	Balanced-FFE	FIESTA	High
Modified SSFP-balanced	CISS		FIESTA-C	High
Spoiled gradient echo	FLASH	T1 FFE	SPGR	Low

Abbreviations: FID = free induction decay; FLAIR = fluid-attenuated inversion recovery; IR = inversion recovery.

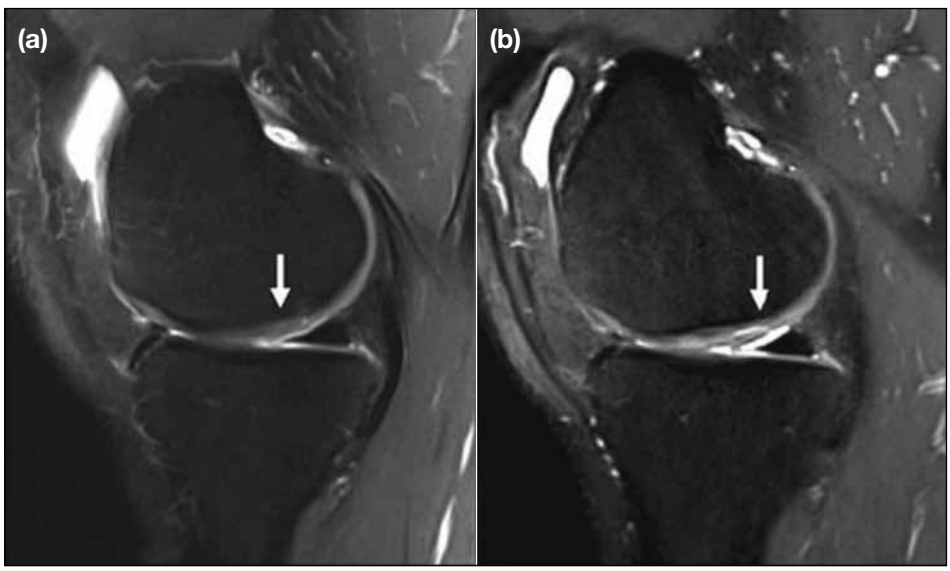

Figure 7. (a) Fat-suppressed sagittal T2-weighted fast spin-echo image showing slight irregularity of the hyaline articular cartilage with a small focal region of intracartilaginous fluid indicative of a small cartilage fissure with intrasubstance joint fluid (arrow). (b) Fat-suppressed three-dimensional isotropic proton density–weighted image showing a moderate-size flap tear of the delaminated articular cartilage with undermining joint fluid (arrow), which is not evident in (a) owing to volume effects. Isotropic three-dimensional fast spin-echo sequences are useful to assess musculoskeletal pathologies (images courtesy of Prof. LM White).

and biomechanical degenerative changes in tissue that are associated with degeneration, remodelling, or healing of the MSK system. Recent research has focused on the MRI biochemical and biomechanical evolution of the cartilage ultrastructure, including changes to the content and organisation of the collagen network, hydration, proteoglycans content, and its distribution.[47,48] Degenerative cartilage is generally associated with decreased proteoglycans concentration, increased water content, and an increased rate of synthesis and degradation of matrix macromolecules.[49] Advanced MRI techniques to detect biochemical and biomechanical changes in cartilage include T2 / T2* mapping, $T_{1\varrho}$ mapping, delayed gadolinium-enhanced MRI of cartilage (dGEMRIC), glycosaminoglycan chemical exchange saturation transfer (gagCEST),[50] and the sodium MRI (Table 3).[50,51] T2 mapping is effective in quantifying changes associated with collagen matrix concentration and organisation and water content because T2 relaxation time depends on the quantity of proteoglycans and water in the articular cartilage. T2 mapping is effective in detecting early physiological changes of osteoarthritis[52,53] in the spine (Figure 8) and knee joint cartilage (Figure 9).

Technical concerns must be taken into account to determine how T2 relaxation time varies with different protocols and parameters. Spin echo imaging with

Table 3. Summary of some advanced magnetic resonance imaging (MRI) techniques for cartilage evaluation.

Technique	Biochemical composition evaluated	Applications and advantages	Drawbacks
T2 mapping	Water content; indirectly for collagen content and orientation	Detect cartilage health without the need for contrast; commercially available	Longer scan time; less sensitive in early stages of cartilage degeneration; T2 variations related to diurnal effects and pulse sequences; magic angle effect
T2* mapping	Water content; indirectly for collagen content and orientation	High spatial resolution; short scan time	Magic angle effect; prone to susceptibility artefacts; not suitable for patients with postsurgical debris or area with tissue interfaces
$T_1\rho$ mapping	Water content; content of cartilage, GAG, and PG	Sensitivity for early cartilage damage	Higher specific absorption rate and potential tissue heating
Diffusion-weighted imaging	Microscopic movement of water at the cellular level	Qualitative and quantitative information at the cellular level for differentiation of normal and pathological tissues and benign and malignant vertebral fractures, and for monitoring tumours post-chemotherapy	Low spatial resolution; long scan time; prone to motion artefacts; geometry distortion
Sodium imaging	Indirectly for GAG concentration and distribution	Detect differences in GAG concentration; sensitivity for early cartilage damage	Special transmitter and receiver coils; low concentration leading to low SNR; high magnetic field and high gradient needed
Delayed gadolinium-enhanced MRI of cartilage	Indirectly for GAG content by fixed charged density because the contrast agent accumulates in an inverse relationship with GAG content	Sensitivity for early cartilage damage; lower T1 indicates reduced GAG content; use of 3D techniques to assess cartilage with a short scan time	Contrast media needed; longer total scan time for contrast uptake
Glycosaminoglycan chemical exchange saturation transfer	GAG content	Provide contrast between regions of high and low GAG content; sensitivity for early cartilage damage	High magnetic field needed; low SNR; susceptibility of the technique to B_0 inhomogeneities; sophisticated post-processing tools needed for complex data analysis
Ultrashort time echo imaging	Tissues with T2 / T2* relaxation time <5 ms include menisci, tendons, ligaments, entheses, and deep radial and calcified layers of cartilage	Enable T2- and T2*-weighted imaging of tissues invisible in a conventional T2 and T2* pulse sequence by using an extremely short echo time	Require specialised equipment; low SNR due to the low concentration of short T2 components

Abbreviations: GAG = glycosaminoglycan; PG = proteoglycan; SNR = signal-to-noise ratio.

separate acquisitions for each echo time provides a standard for clinical T2 relaxation time measurement. Multi echo spin echo, fast spin echo, and the gradient and spin-echo sequences are developed to reduce overall scan time.[54-56] T2 relaxation time quantification can be affected by T1 saturation effects, imperfect radiofrequency pulses, static field inhomogeneity, stimulated echoes, and insufficient sampling of the T2 decay points. Therefore, it is essential to select the appropriate T2 mapping protocols and perform proper postprocessing exponential fit when attempting to measure T2 relaxation time.

ULTRASHORT ECHO-TIME IMAGING

Conventional T1- and T2-weighted pulse sequences with echo times ranging from 2-200 ms are effective for clinical examinations. Nonetheless, for tissues with very short T2s ranging from hundreds of microseconds to tens of milliseconds such as tendons, ligaments, and menisci (Table 4), conventional sequences derive little or no signal from these tissue components.[57] Ultrashort echo-time (UTE) sequences are initially designed to detect signals from tissues with very short T2s in the MSK system. The UTE pulse sequences use half radiofrequency excitations with radial sampling from the centre of k-space.[58] UTE sequences are implemented with TEs 10 to 50 times shorter than those of routine clinical imaging sequences to obtain a high signal for tissues with short T2s. UTE sequences are applied in various areas of clinical practice, especially for the MSK system, and can differentiate zones of the meniscus, visualise layers and defects of articular cartilage, and enhance ligamentous scar tissue (Figure 10). Nonetheless, the low SNR due to the low concentration of short T2 components in many tissues is a concern, as

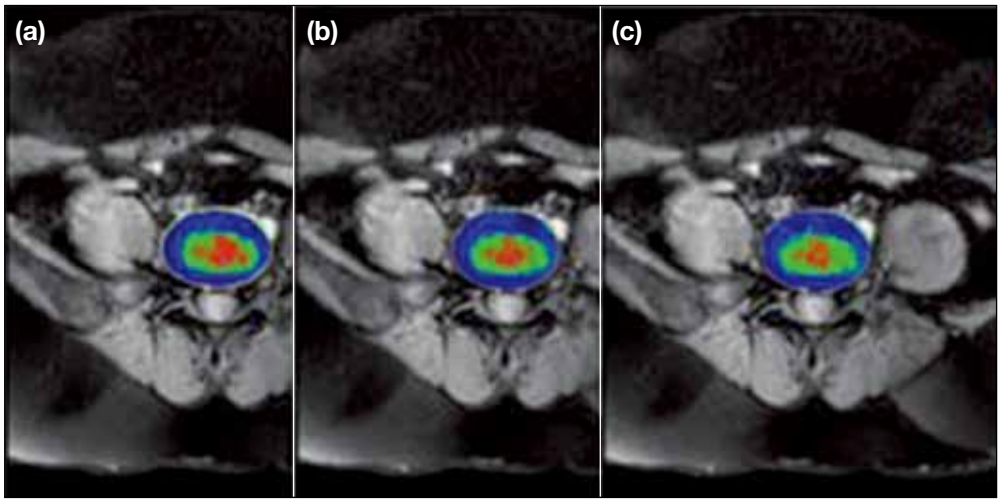

Figure 8. T2 mapping is sensitive to detect small variations in disc content over time and is useful to observe early physiological changes of osteoarthritis.

Figure 9. Quantitative imaging of the knee joint cartilage with T2 mapping.

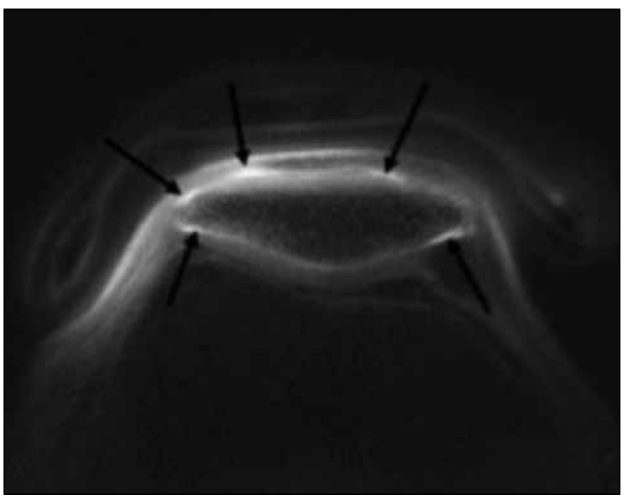

Figure 10. A transverse fat-suppressed ultrashort echo-time (TE = 0.08 ms at 1.5 T) image of the patellar showing a high signal (arrows) in the calcified tissue (image courtesy of Dr. Damian J. Tyler).

Table 4. T2 relaxation time for very short T2 tissue components from adults.

Tissue	Mean T2 relaxation time estimated for 1.5 T (ms)
Ligaments	4-10
Tendon	4-7
Menisci	5-8
Cortical bone	0.4-0.5
Periosteum	5-11
Protons in proteins	0.01
Protons in solids	0.001

is patient motion. Despite these, UTE sequences enable visualisation of previously 'invisible' tissues and tissue components as well as characterisation of MSK tissues.

CONCLUSION

MRI enables a comprehensive, non-invasive, and non-ionising evaluation of the MSK system. Imaging quality and characteristics such as imaging resolution, speed, and SNR have been improved due to technical advances in coil technology and high-field scanners.

New MRI techniques including T2 and $T_{1\rho}$ mapping, diffusion-weighted and tensor imaging,[59] sodium imaging, MR spectroscopy, and ultrashort TE imaging are advanced techniques that enable quantitative and non-invasive monitoring of the maturation of repaired tissue following microfracture surgery and evaluation of earlier stages of pathology in MSK tissue. Nonetheless, pulse sequences should be modified and optimised to achieve their full clinical potential, as should advances in both hardware and software technology.

REFERENCES

1. Roemer PB, Edelstein WA, Hayes CE, Souza SP, Mueller OM. The NMR phased array. Magn Reson Med. 1990;16:192-225. cross ref
2. Pruessmann KP, Weiger M, Scheidegger MB, Boesiger P. SENSE: sensitivity encoding for fast MRI. Magn Reson Med. 1999;42:952-62. cross ref
3. Sodickson DK, Manning WJ. Simultaneous acquisition of spatial harmonics (SMASH): fast imaging with radiofrequency coil arrays. Magn Reson Med. 1997;38:591-603. cross ref
4. Griswold MA, Jakob PM, Heidemann RM, Nittka M, Jellus V, Wang J, et al. Generalized autocalibrating partially parallel acquisitions (GRAPPA). Magn Reson Med. 2002;47:1202-10. cross ref
5. Zhu Y, Hardy CJ, Sodickson DK, Giaquinto RO, Dumoulin CL, Kenwood G, et al. Highly parallel volumetric imaging with a 32-element RF coil array. Magn Reson Med. 2004;52:869-77. cross ref
6. Mosher TJ. Musculoskeletal imaging at 3T: current techniques and future applications. Magn Reson Imaging Clin N Am. 2006;14:63-76. cross ref
7. Ramnath RR. 3T MR imaging of the musculoskeletal system (Part I): considerations, coils, and challenges. Magn Reson Imaging Clin N Am. 2006;14:27-40. cross ref
8. Ramnath RR. 3T MR imaging of the musculoskeletal system (Part II): clinical applications. Magn Reson Imaging Clin N Am. 2006;14:41-62. cross ref
9. Schmitt F, Grosu D, Mohr C, Purdy D, Salem K, Scott KT, et al. 3 Tesla MRI: successful results with higher field strengths [in German]. Radiologe. 2004;44:31-47.
10. Mosher TJ. MRI of osteochondral injuries of the knee and ankle in the athlete. Clin Sports Med. 2006;25:843-66. cross ref
11. Mosher TJ, Davis CM 3rd. Magnetic resonance imaging to evaluate osteolysis around total knee arthroplasty. J Arthroplasty. 2006;21:460-3. cross ref
12. Ramnath RR, Magee T, Wasudev N, Murrah R. Accuracy of 3-T MRI using fast spin-echo technique to detect meniscal tears of the knee. AJR Am J Roentgenol. 2006;187:221-5. cross ref
13. Schmidt GP, Reiser MF, Baur-Melnyk A. Whole-body imaging of the musculoskeletal system: the value of MR imaging. Skeletal Radiol. 2007;36:1109-19. cross ref
14. Schmidt GP, Wintersperger B, Graser A, Baur-Melnyk A, Reiser MF, Schoenberg SO. High-resolution whole-body magnetic resonance imaging applications at 1.5 and 3 Tesla: a comparative study. Invest Radiol. 2007;42:449-59. cross ref
15. Schmidt GP, Schoenberg SO, Schmid R, Stahl R, Tiling R, Becker CR, et al. Screening for bone metastases: whole-body MRI using a 32-channel system versus dual-modality PET-CT. Eur Radiol. 2007;17:939-49. cross ref
16. Kurtz S, Mowat F, Ong K, Chan N, Lau E, Halpern M. Prevalence of primary and revision total hip and knee arthroplasty in the United States from 1990 through 2002. J Bone Joint Surg Am. 2005;87:1487-97. cross ref
17. Schenck JF. The role of magnetic susceptibility in magnetic resonance imaging: MRI magnetic compatibility of the first and second kinds. Med Phys. 1996;23:815-50. cross ref
18. Port JD, Pomper MG. Quantification and minimization of magnetic susceptibility artifacts on GRE images. J Comput Assist Tomogr. 2000;24:958-64. cross ref
19. Eustace S, Goldberg R, Williamson D, Melhem ER, Oladipo O, Yucel EK, et al. MR imaging of soft tissues adjacent to orthopaedic hardware: techniques to minimize susceptibility artefact. Clin Radiol. 1997;52:589-94. cross ref
20. Lee MJ, Kim S, Lee SA, Song HT, Huh YM, Kim DH, et al. Overcoming artifacts from metallic orthopedic implants at high-field-strength MR imaging and multi-detector CT. Radiographics. 2007;27:791-803. cross ref
21. Keller PJ, Hunter WW Jr, Schmalbrock P. Multisection fat-water imaging with chemical shift selective presaturation. Radiology. 1987;164:539-41. cross ref
22. Dixon WT. Simple proton spectroscopic imaging. Radiology. 1984;153:189-94. cross ref
23. Glover GH, Schneider E. Three-point Dixon technique for true water/fat decomposition with B0 inhomogeneity correction. Magn Reson Med. 1991;18:371-83. cross ref
24. Glover GH. Multipoint Dixon technique for water and fat proton and susceptibility imaging. J Magn Reson Imaging. 1991;1:521-30. cross ref
25. Bydder GM, Young IR. MR imaging: clinical use of the inversion recovery sequence. J Comput Assist Tomogr. 1985;9:659-75. cross ref
26. Cha JG, Jin W, Lee MH, Kim DH, Park JS, Shin WH, et al. Reducing metallic artifacts in postoperative spinal imaging: usefulness of IDEAL contrast-enhanced T1- and T2-weighted MR imaging--phantom and clinical studies. Radiology. 2011;259:885-93. cross ref
27. Cho ZH, Kim DJ, Kim YK. Total inhomogeneity correction including chemical shifts and susceptibility by view angle tilting. Med Phys. 1988;15:7-11. cross ref
28. Olsen RV, Munk PL, Lee MJ, Janzen DL, MacKay AL, Xiang QS, et al. Metal artifact reduction sequence: early clinical applications. Radiographics. 2000;20:699-712. cross ref
29. Lu W, Pauly KB, Gold GE, Pauly JM, Hargreaves BA. SEMAC: Slice Encoding for Metal Artifact Correction in MRI. Magn Reson Med. 2009;62:66-76. cross ref
30. Koch KM, Lorbiecki JE, Hinks RS, King KF. A multispectral three-dimensional acquisition technique for imaging near metal implants. Magn Reson Med. 2009;61:381-90. cross ref
31. Sonin AH, Pensy RA, Mulligan ME, Hatem S. Grading articular cartilage of the knee using fast spin-echo proton density-weighted MR imaging without fat suppression. AJR Am J Roentgenol. 2002;179:1159-66. cross ref
32. Bredella MA, Tirman PF, Peterfy CG, Zarlingo M, Feller JF, Bost FW, et al. Accuracy of T2-weighted fast spin-echo MR imaging with fat saturation in detecting cartilage defects in the knee: comparison with arthroscopy in 130 patients. AJR Am J Roentgenol. 1999;172:1073-80. cross ref
33. Jee WH, McCauley TR, Kim JM, Jun DJ, Lee YJ, Choi BG, et al. Meniscal tear configurations: categorization with MR imaging. AJR Am J Roentgenol. 2003;180:93-7. cross ref
34. Schaefer FK, Schaefer PJ, Brossmann J, Frahm C, Muhle C, Hilgert RE, et al. Value of fat-suppressed PD-weighted TSE-sequences

for detection of anterior and posterior cruciate ligament lesions--comparison to arthroscopy. Eur J Radiol. 2006;58:411-5. cross ref
35. Duc SR, Zanetti M, Kramer J, Kach KP, Zollikofer CL, Wentz KU. Magnetic resonance imaging of anterior cruciate ligament tears: evaluation of standard orthogonal and tailored paracoronal images. Acta Radiol. 2005;46:729-33. cross ref
36. Robinson G, Chung T, Finlay K, Friedman L. Axial oblique MR imaging of the intrinsic ligaments of the wrist: initial experience. Skeletal Radiol. 2006;35:765-73. cross ref
37. Sutherland JK, Nozaki T, Kaneko Y, J Yu H, Rafijah G, Hitt D, et al. Initial experience with 3D isotropic high-resolution 3 T MR arthrography of the wrist. BMC Musculoskelet Disord. 2016;17:30. cross ref
38. Naraghi A, White LM. Three-dimensional MRI of the musculoskeletal system. AJR Am J Roentgenol. 2012;199:W283-93. cross ref
39. Glaser C, Faber S, Eckstein F, Fischer H, Springer V, Heudorfer L, et al. Optimization and validation of a rapid high-resolution T1-w 3D FLASH water excitation MRI sequence for the quantitative assessment of articular cartilage volume and thickness. Magn Reson Imaging. 2001;19:177-85. cross ref
40. Knuesel PR, Pfirrmann CW, Noetzli HP, Dora C, Zanetti M, Hodler J, et al. MR arthrography of the hip: diagnostic performance of a dedicated water-excitation 3D double-echo steady-state sequence to detect cartilage lesions. AJR Am J Roentgenol. 2004;183:1729-35. cross ref
41. Gold GE, Hargreaves BA, Reeder SB, Block WF, Kijowski R, Vasanawala SS, et al. Balanced SSFP imaging of the musculoskeletal system. J Magn Reson Imaging. 2007;25:270-8. cross ref
42. Gold GE, Busse RF, Beehler C, Han E, Brau AC, Beatty PJ, et al. Isotropic MRI of the knee with 3D fast spin-echo extended echo-train acquisition (XETA): initial experience. AJR Am J Roentgenol. 2007;188:1287-93. cross ref
43. Busse RF, Brau AC, Vu A, Michelich CR, Bayram E, Kijowski R, et al. Effects of refocusing flip angle modulation and view ordering in 3D fast spin echo. Magn Reson Med. 2008;60:640-9. cross ref
44. Busse RF, Hariharan H, Vu A, Brittain JH. Fast spin echo sequences with very long echo trains: design of variable refocusing flip angle schedules and generation of clinical T2 contrast. Magn Reson Med. 2006;55:1030-7. cross ref
45. Notohamiprodjo M, Horng A, Pietschmann MF, Muller PE, Horger W, Park J, et al. MRI of the knee at 3T: first clinical results with an isotropic PDfs-weighted 3D-TSE-sequence. Invest Radiol. 2009;44:585-97. cross ref
46. Ristow O, Steinbach L, Sabo G, Krug R, Huber M, Rauscher I, et al. Isotropic 3D fast spin-echo imaging versus standard 2D imaging at 3.0 T of the knee--image quality and diagnostic performance. Eur Radiol 2009;19:1263-72. cross ref
47. Nishii T, Tanaka H, Sugano N, Sakai T, Hananouchi T, Yoshikawa H. Evaluation of cartilage matrix disorders by T2 relaxation time in patients with hip dysplasia. Osteoarthritis Cartilage. 2008;16:227-33. cross ref
48. Nishii T, Kuroda K, Matsuoka Y, Sahara T, Yoshikawa H. Change in knee cartilage T2 in response to mechanical loading. J Magn Reson Imaging. 2008;28:175-80. cross ref
49. Xia Y. Magic-angle effect in magnetic resonance imaging of articular cartilage: a review. Invest Radiol. 2000;35:602-21. cross ref
50. Ling W, Regatte RR, Navon G, Jerschow A. Assessment of glycosaminoglycan concentration in vivo by chemical exchange-dependent saturation transfer (gagCEST). Proc Natl Acad Sci U S A. 2008;105:2266-70. cross ref
51. Madelin G, Regatte RR. Biomedical applications of sodium MRI in vivo. J Magn Reson Imaging. 2013;38:511-29. cross ref
52. Poon CS, Henkelman RM. Practical T2 quantitation for clinical applications. J Magn Reson Imaging. 1992;2:541-53. cross ref
53. Mosher TJ, Smith H, Dardzinski BJ, Schmithorst VJ, Smith MB. MR imaging and T2 mapping of femoral cartilage: in vivo determination of the magic angle effect. AJR Am J Roentgenol. 2001;177:665-9. cross ref
54. Mosher TJ, Dardzinski BJ. Cartilage MRI T2 relaxation time mapping: overview and applications. Semin Musculoskelet Radiol. 2004;8:355-68. cross ref
55. Oshio K, Feinberg DA. GRASE (Gradient- and spin-echo) imaging: a novel fast MRI technique. Magn Reson Med. 1991;20:344-9. cross ref
56. Mendlik T, Faber SC, Weber J, Hohe J, Rauch E, Reiser M, Glaser C. T2 quantitation of human articular cartilage in a clinical setting at 1.5 T: implementation and testing of four multiecho pulse sequence designs for validity. Invest Radiol. 2004;39:288-99. cross ref
57. Reichert IL, Robson MD, Gatehouse PD, He T, Chappell KE, Holmes J, et al. Magnetic resonance imaging of cortical bone with ultrashort TE pulse sequences. Magn Reson Imaging. 2005;23:611-8. cross ref
58. Nielsen HT, Gold GE, Olcott EW, Pauly JM, Nishimura DG. Ultra-short echo-time 2D time-of-flight MR angiography using a half-pulse excitation. Magn Reson Med. 1999;41:591-9. cross ref
59. Subhawong TK, Jacobs MA, Fayad LM. Insights into quantitative diffusion-weighted MRI for musculoskeletal tumor imaging. AJR Am J Roentgenol. 2014;203:560-72. cross ref